Eur. Phys. J. AP **5**, 143–148 (1999)

THE EUROPEAN PHYSICAL JOURNAL APPLIED PHYSICS

Backscattering of electrons from selected oxides: MgO, SiO_2, and Al_2O_3

M. Dapor[1,a] and A. Miotello[2]

[1] Advanced Materials Division, ITC and INFM, 38050 Povo, Trento, Italy
[2] INFM and Physics Department, Trento University, 38050 Povo, Trento, Italy

Received: 7 August 1998 / Revised: 5 November 1998 / Accepted: 19 November 1998

Abstract. The inelastic and elastic cross-sections of an interacting electron beam with MgO, SiO_2, and Al_2O_3 have been calculated and tabulations are provided for primary electron energies lower than 10 keV. By using the tabulated cross-sections, a Monte-Carlo simulation is utilized to obtain the backscattering coefficient in the energy range 1–10 keV

PACS. 72.20.Dp General theory, scattering mechanisms – 79.20.-m Impact phenomena (including electron spectra and sputtering)

1 Introduction

Electron beams are widely utilized in microanalytical techniques such as Auger electron spectroscopy, transmission electron microscopy, electron-probe microanalysis, and electron-beam lithography. The problem of an accurate calculation of the inelastic and elastic scattering cross-sections of low to medium energy (50 eV–10 keV) electrons interacting with insulators is of great interest both in applied fields where oxides are possibly utilized as radiation-resistant materials and in connection with the use of Monte-Carlo simulations to study the interaction of electron beams with dielectric materials. Indeed, both Monte-Carlo simulations and analytical methods utilized to analyze the electron-solid (-atom) interaction require an accurate knowledge of the scattering cross-sections, stopping power, and mean free paths. Unfortunately, the cross-sections of charged particles interacting with atoms, particularly for low to medium kinetic energies, are not computable by using simple closed formulas.

In each collisional event with an atomic electron or a nucleus, the incident electron both loses energy and changes its propagation direction. The incident electrons lose energy mainly through atomic-electron excitation or ejection and plasmon excitation. These inelastic scattering processes also influence the electron trajectory in the solid but in a rather weak way, at least when the electron energy is not too low. Since in our Monte-Carlo calculations concerning backscattering the primary energies are in the range 1–10 keV, the angular deflections due to inelastic scattering can be safely neglected. The nuclear collisions, on the other hand, due to the large mass difference between the electron and the atomic nucleus, are nearly elastic: they strongly affect the direction of the incident particle in the solid without substantial energy transfer.

The inelastic scattering can be quantified by utilizing the inelastic mean-free path and the stopping power, a quantity related to the probability of energy loss per unit distance traveled by the electron inside the solid. An electron can lose a large fraction of its energy in a single collision: nevertheless, the so-called continuous slowing down approximation is, generally, accepted. In this approximation, the electron is assumed to continuously dissipate its energy while traveling inside the solid. We calculated the inelastic mean-free paths and stopping power by following the method proposed by Ashley [1] and utilizing the mass absorption coefficients reported by Henke *et al.* [2], as illustrated in the following section.

The elastic scattering cross-sections can be obtained by calculating the phase shifts. Since the large-r asymptotic behavior (r is the radial coordinate) of the radial wave function is known, the phase shifts can be computed by numerically solving the Dirac equation for a central electrostatic field up to values of r where the atomic potential can be safely neglected. This method was proposed by Lin *et al.* [3] and developed by Bunyan and Schonfelder [4]. The differential cross-section thus obtained is generally known as the Mott cross-section [5].

In this paper the inelastic and elastic cross-sections for an electron beam interacting with MgO, SiO_2, and Al_2O_3 have been calculated and tabulations are provided for primary electron energies up to 10 keV.

The tabulated values of the elastic and inelastic cross-sections are utilized in a Monte-Carlo simulation to calculate the backscattering coefficient of electrons in the energy range 1–10 keV for the three selected oxides.

[a] e-mail: dapor@itc.it

2 Inelastic scattering

Ashley [1] has shown that the inelastic mean free path and the stopping power of slow electrons penetrating in solid targets may be computed, respectively, by using the following equations:

$$\lambda_{inel}^{-1} = \frac{me^2}{2\pi\hbar^2 E} \int_0^{E/2} \mathrm{Im}\left[\frac{-1}{\varepsilon(0,\omega)}\right] L_e\left(\frac{\hbar\omega}{E}\right) d(\hbar\omega), \quad (1)$$

$$-\frac{dE}{ds} = \frac{me^2}{\pi\hbar^2 E} \int_0^{E/2} \mathrm{Im}\left[\frac{-1}{\varepsilon(0,\omega)}\right] G_e\left(\frac{\hbar\omega}{E}\right) \hbar\omega d(\hbar\omega). \quad (2)$$

In these equations m is the electron mass, e is the electron charge, h is the Planck constant, E is the incident electron energy, s is the trajectory coordinate and $\varepsilon(0,\omega) = \varepsilon(k = 0,\omega)$ is the dielectric constant. Here k is the momentum transfered while ω is the energy transfered. Note that in equations (1, 2) $k = 0$ because the ε dependence on k was factorized through the functions L_e and G_e.

The functions L_e and G_e may be approximated by [1]

$$L_e(x) = (1-x)\ln\frac{4}{x} - \frac{7}{4}x + x^{3/2} - \frac{33}{32}x^2, \quad (3)$$

$$G_e(x) = \ln\frac{1.166}{x} - \frac{3}{4}x - \frac{x}{4}\ln\frac{4}{x} + \frac{1}{2}x^{3/2} - \frac{x^2}{16}\ln\frac{4}{x} - \frac{31}{48}x^2. \quad (4)$$

For further details about the factorization procedure see reference [1]. Note that exchange effects are included, in an approximate way, in equations (1, 2).

The function $\mathrm{Im}\{-1/[\varepsilon(0,\omega)]\}$ is the optical-loss function which can be calculated from optical data. It is given by

$$\mathrm{Im}\left[\frac{-1}{\varepsilon(0,\omega)}\right] = \frac{\varepsilon_2}{\varepsilon_1^2 + \varepsilon_2^2}, \quad (5)$$

where

$$\varepsilon = \varepsilon_1 + i\varepsilon_2, \quad (6)$$

$$\varepsilon_1 = n^2 - k^2, \quad (7)$$

$$\varepsilon_2 = 2nk, \quad (8)$$

and the index of refraction n and the extinction coefficient k are given by [2]

$$n = 1 - \frac{e^2}{2\pi m\ c^2}\lambda^2 N \sum_p x_p f_{1p}, \quad (9)$$

$$k = \frac{e^2}{2\pi m\ c^2}\lambda^2 N \sum_p x_p f_{2p}. \quad (10)$$

In these equations c is the speed of light, N the number of molecules per unit volume each having x_p atoms, λ the photon wavelength, and f_{1p} and f_{2p} are the real and the imaginary components of the atomic scattering factor, respectively. The calculation of the real and imaginary components of the atomic scattering factor has been performed by using the following equations [2]

$$f_1 = Z + \frac{mc^2}{2\pi^2\hbar ce^2}\frac{A}{N_A}\int_0^\infty \frac{\epsilon^2\mu(\epsilon)}{E_p^2 - \epsilon^2}d\epsilon, \quad (11)$$

$$f_2 = \frac{mc^2}{4\pi\hbar ce^2}\frac{A}{N_A}E_p\mu(E_p). \quad (12)$$

In these equations E_p is the incident photon energy, Z the atomic number, A the atomic weight, N_A the Avogadro's number and μ the photoabsorption cross-section (cm^2/g). In conclusion our calculations will be performed from tabulations of the mass absorption coefficient μ [2] from which, as indicated by equations (9–12) the optical loss function is derived and then utilized in equations (1, 2) to give the inelastic mean free path and the stopping power. The Henke *et al.* data [2] are given for discrete photon energies (beginning at 30.5 eV and then 49.3 eV, 72.4 eV and so on) and, thus, we performed the calculation of the optical loss function utilizing a cubic spline interpolation of the mass absorption coefficients. Since the Henke *et al.* data [2] begin at 30.5 eV, we performed polynomial extrapolation of their data to calculate the mass absorption coefficients for energies lower than 30.5 eV. We are interested in compound materials and then, once calculated the real and imaginary parts of the atomic scattering factor for the single elements constituting the oxides, by using equations (11, 12), we calculate n and k for each oxide by utilizing equations (9, 10), as suggested by Henke *et al.* [2]: in fact, following these authors, for the low-energy photon region it is reasonable to assume that "the atoms within a condensed system [...] act independently as scattering dipoles" and that "the total atomic dipole moment per unit electric field is proportional to the average atomic scattering factor for the medium". In conclusion, the values of n and k relative to the oxides obtained in this way will be introduced in equations (7, 8). Then, by using equation (5), the optical loss function for the oxide will be obtained and utilized for the computation of the inelastic mean free path and stopping power (Eqs. (1, 2)). Despite the mentioned approximations, which have been included into the optical loss function calculation, our evaluation of the accuracy of the inelastic mean free path and stopping power is $\sim$ 1–5%: our inelastic mean free path and stopping power calculations, as we will show below, agree reasonably well with the results of other authors and very well with the available experimental data.

The extrapolation procedure we used to get the loss function is admittedly approximate, and nevertheless we obtained good agreement with the available experimental data. This is due to the fact that both inelastic mean free path and stopping power are integrated quantities.

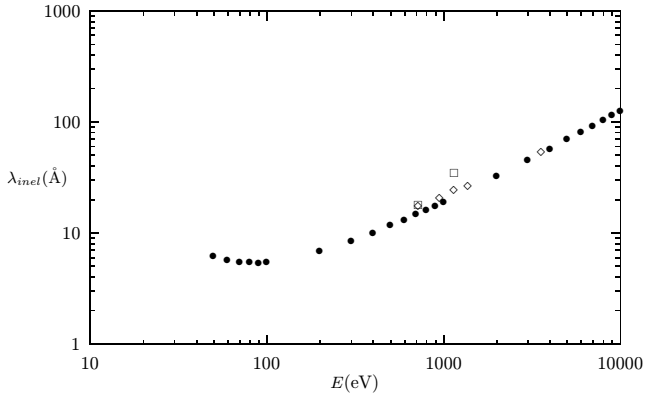

Fig. 1. Electron inelastic mean-free path in SiO_2 as a function of the primary electron energy. (•) This work; (◇) experimental data of Flitsch and Raider [11]; (□) experimental data of Ishizaka *et al.* [12].

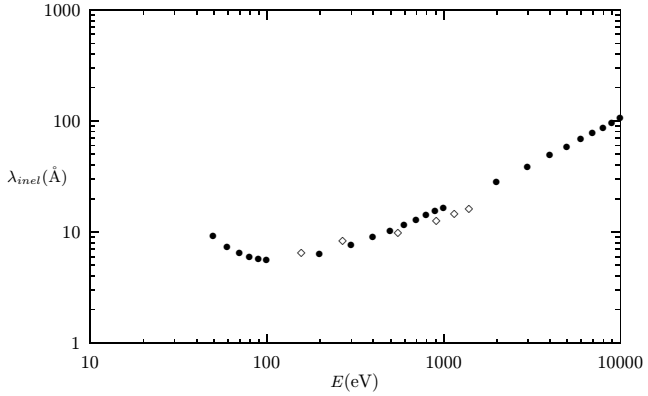

Fig. 2. Electron inelastic mean-free path in Al_2O_3 as a function of the primary electron energy. (•), this work; (◇), experimental data of Battye *et al.* [10].

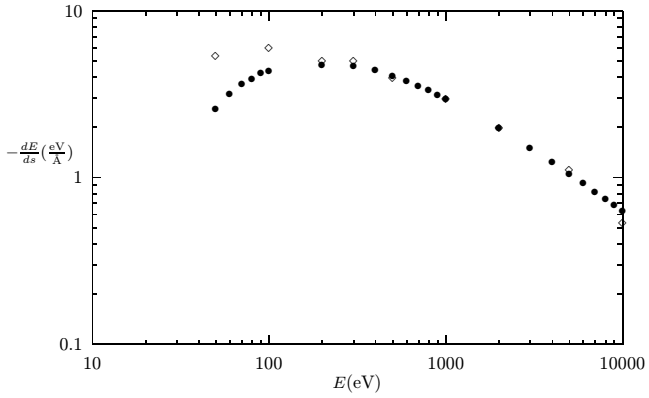

Fig. 3. Electron stopping power in MgO as a function of the primary electron energy. (•), this work; (◇), experimental data reported by Akkerman *et al.* [14] taken from the Joy's data base [15].

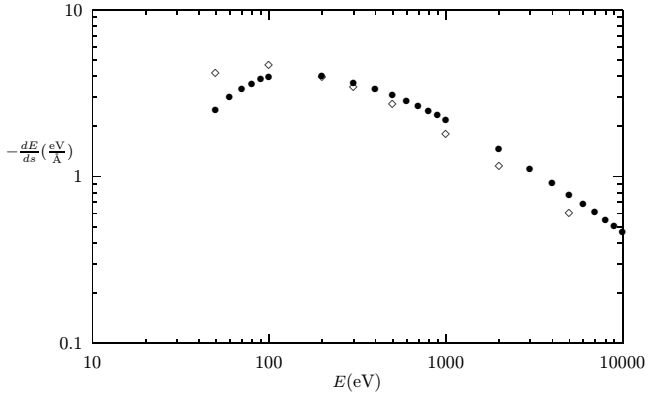

Fig. 4. Electron stopping power in SiO_2 as a function of the primary electron energy. (•), this work; (◇), experimental data reported by Akkerman *et al.* [14] taken from the Joy's data base [15].

To compare our results for the stopping power at high energy with the Bethe formula, we need the value of the mean ionization energy I. By using the value given by Pages *et al.* [7], namely $I = 142$ eV for SiO_2, for example, the stopping power at 10 keV obtained with the Bethe formula is 0.458 eV/Å. Our stopping power at 10 keV is 0.462 eV/Å, higher by 0.9% compared to Bethe's value. Note that the 10 keV stopping power of Ashley and Anderson is 0.461 eV/Å [8]. For the range of primary energies utilized here for Monte-Carlo simulation of the backscattering coefficient, the structure of the loss function can be safely neglected and the integrated quantities are sufficiently accurate.

3 Elastic scattering

The differential elastic-scattering cross-section is given by:

$$\frac{d\sigma}{d\Omega} = \mid f \mid^2 + \mid g \mid^2 , \tag{13}$$

where the direct and spin-flip scattering amplitudes $f(\theta)$ and $g(\theta)$ (θ = the polar scattering angle with respect to the incidence direction) are given by [5]:

$$f(\theta) = \frac{1}{2iK} \sum_{l=0}^{\infty} \Big\{ (l+1)[\exp(2i\delta_l^-) - 1] + l[\exp(2i\delta_l^+) - 1] \Big\} P_l(\cos\theta), \tag{14}$$

$$g(\theta) = \frac{1}{2iK} \sum_{l=1}^{\infty} \left[-\exp(2i\delta_l^-) + \exp(2i\delta_l^+) \right] P_l^1(\cos\theta). \tag{15}$$

In these equations, $K^2 = (E^2 - m^2c^4)/\hbar^2c^2$, $\hbar K$ is the momentum of the electron incident on the atom, E the total energy, m the electron mass, c the speed of light, P_l are Legendre's polynomials, and

$$P_l^1(x) = (1 - x^2)^{1/2} \frac{dP_l(x)}{dx} \cdot \tag{16}$$

Table 1. Electron inelastic mean free path (Å) in MgO, SiO_2, and Al_2O_3.

E (eV)	MgO	SiO_2	Al_2O_3
50	7.27	6.39	9.08
60	6.33	5.87	7.22
70	5.91	5.64	6.39
80	5.72	5.55	5.96
90	5.62	5.51	5.67
100	5.63	5.57	5.58
150	6.08	6.18	5.79
200	6.70	7.00	6.35
250	7.36	7.84	6.97
300	8.05	8.69	7.61
400	9.44	10.3	8.92
500	10.8	12.0	10.2
600	12.2	13.5	11.5
700	13.5	15.1	12.7
800	14.8	16.6	14.0
900	16.1	18.1	15.2
1 000	17.4	19.6	16.4
1 500	23.6	26.8	22.2
2 000	29.6	33.6	27.8
2 500	35.3	40.2	33.2
3 000	40.9	46.6	38.4
4 000	51.7	59.1	48.6
5 000	62.2	71.2	58.4
6 000	72.4	83.0	68.0
7 000	82.5	94.6	77.4
8 000	92.3	106	86.6
9 000	102	117	95.7
10 000	112	128	105

Table 2. Stopping power (eV/Å) of electrons in MgO, SiO_2, and Al_2O_3.

E (eV)	MgO	SiO_2	Al_2O_3
50	2.56	2.50	2.43
60	3.17	2.98	3.23
70	3.60	3.33	3.85
80	3.90	3.58	4.32
90	4.19	3.84	4.79
100	4.32	3.96	5.04
150	4.63	4.14	5.48
200	4.74	3.97	5.42
250	4.74	3.79	5.30
300	4.65	3.62	5.13
400	4.37	3.32	4.76
500	4.07	3.06	4.42
600	3.79	2.83	4.11
700	3.54	2.63	3.83
800	3.32	2.46	3.59
900	3.13	2.32	3.37
1 000	2.95	2.18	3.19
1 500	2.34	1.73	2.52
2 000	1.96	1.45	2.11
2 500	1.69	1.25	1.83
3 000	1.49	1.11	1.62
4 000	1.23	0.907	1.33
5 000	1.05	0.774	1.13
6 000	0.919	0.678	0.992
7 000	0.820	0.605	0.885
8 000	0.743	0.547	0.801
9 000	0.680	0.501	0.733
10 000	0.627	0.462	0.677

The phase shifts δ_l^- and δ_l^+ can be computed by using the equation (*cf.*, for example [18,20])

$$\tan\delta_l^{\pm} = \frac{Kj_{l+1}(Kr) - j_l(Kr)[\zeta\tan\phi_l^{\pm} + (1+l+k^{\pm})/r]}{Kn_{l+1}(Kr) - n_l(Kr)[\zeta\tan\phi_l^{\pm} + (1+l+k^{\pm})/r]}, \tag{17}$$

where

$$\zeta = \frac{E+mc^2}{\hbar c}\,. \tag{18}$$

In equation (17), $k^+ = -l-1$, and $k^- = l$, j_l are the regular-spherical Bessel functions, and n_l the irregular-spherical Bessel functions. $\phi_l^{\pm}$ has to be computed as:

$$\phi_l^{\pm} = \lim_{r\to\infty}\phi_l^{\pm}(r), \tag{19}$$

where $\phi_l^{\pm}(r)$ is the solution of the Dirac's equation which can be reduced, as shown by Lin, Sherman, and Percus [3] and by Bunyan and Schonfelder [4], to the first-order differential equation:

$$\frac{d\phi_l^{\pm}(r)}{dr} = \frac{k^{\pm}}{r}\sin[2\phi_l^{\pm}(r)] - \frac{mc^2}{\hbar c}\cos[2\phi_l^{\pm}(r)] + \frac{E-V(r)}{\hbar c}\,. \tag{20}$$

Here, $V(r)$ is the electron-atom potential (calculated within the Hartree-Fock approximation).

Since electrons are identical particles, exchange effects were taken into account by adding the Furness and McCarthy expression [6] to the potential energy describing the electron atom interaction: indeed, it may occur that the incident electron is captured by an atom with emission of a new electron.

The differential-elastic scattering cross-section, in molecular solids, can be approximated by using the additivity rule, *i.e.* the sum of the atomic differential elastic scattering cross-sections of all atoms in the molecule.

The use of the additivity rule in polar molecules may be problematic because such a rule uses phase shifts calculated for independent atoms. This problem was addressed by Baró *et al.* [9]: they concluded that the additivity rule works with sufficient accuracy for the Monte-Carlo simulation purposes allowing, on the other hand, a considerable simplification of the calculation.

Once the differential-elastic scattering cross-section is known, the calculation of the total-elastic scattering cross-section, σ_{el}, and of the momentum transfer (or transport) cross-section, σ_{tr}, may be performed with the following equations:

$$\sigma_{el} = 2\pi\int_0^{\pi}\frac{d\sigma}{d\Omega}\sin\theta d\theta, \tag{21}$$

Table 3. Total elastic scattering cross-section (Å^2) of electrons impinging on MgO, SiO_2, and Al_2O_3.

E (eV)	MgO	SiO_2	Al_2O_3
50	8.21	13.8	22.9
60	7.52	12.3	20.7
70	6.99	11.3	19.2
80	6.56	10.5	17.9
90	6.19	9.86	16.9
100	5.88	9.35	16.1
150	4.76	7.61	13.1
200	4.06	6.54	11.2
250	3.56	5.78	9.84
300	3.19	5.20	8.82
400	2.67	4.38	7.39
500	2.31	3.80	6.40
600	2.05	3.38	5.66
700	1.85	3.04	5.10
800	1.68	2.77	4.64
900	1.55	2.55	4.27
1 000	1.44	2.37	3.96
1 500	1.06	1.75	2.92
2 000	0.845	1.40	2.33
2 500	0.704	1.17	1.94
3 000	0.604	1.01	1.67
4 000	0.472	0.788	1.30
5 000	0.388	0.649	1.07
6 000	0.330	0.553	0.913
7 000	0.287	0.482	0.794
8 000	0.254	0.428	0.704
9 000	0.228	0.385	0.633
10 000	0.207	0.350	0.575

Table 4. Transport elastic scattering cross-section (Å^2) of electrons impinging on MgO, SiO_2, and Al_2O_3.

E (eV)	MgO	SiO_2	Al_2O_3
50	5.62	9.00	14.7
60	4.93	7.87	12.9
70	4.36	6.95	11.4
80	3.89	6.19	10.1
90	3.51	5.56	9.10
100	3.18	5.02	8.23
150	2.09	3.26	5.37
200	1.51	2.33	3.84
250	1.14	1.77	2.92
300	0.906	1.39	2.31
400	0.617	0.946	1.57
500	0.451	0.692	1.15
600	0.347	0.532	0.881
700	0.277	0.424	0.703
800	0.227	0.348	0.575
900	0.190	0.291	0.481
1 000	0.161	0.248	0.410
1 500	0.085 3	0.131	0.217
2 000	0.053 6	0.082 4	0.136
2 500	0.037 0	0.057 0	0.094 1
3 000	0.027 2	0.042 1	0.069 3
4 000	0.016 7	0.025 9	0.042 5
5 000	0.011 3	0.017 6	0.029 0
6 000	0.008 26	0.012 9	0.021 1
7 000	0.006 31	0.009 83	0.016 1
8 000	0.004 99	0.007 78	0.012 8
9 000	0.004 05	0.006 33	0.010 4
10 000	0.003 36	0.005 25	0.008 61

$$\sigma_{tr} = 2\pi \int_0^{\pi} (1 - \cos\theta) \frac{d\sigma}{d\Omega} \sin\theta d\theta. \qquad (22)$$

Since we are interested in compound materials, the elastic scattering cross-sections (differential, total and transport) will be calculated by weighted sums of the cross-sections for the single elements constituting the oxide.

4 Results and discussion

One of the more efficient computational technique utilized to better understand the phenomena which occur when electrons penetrate solid targets (backscattering, secondary electron-emission, charging effects, and so on) is Monte-Carlo simulation. This numerical procedure is very powerful but it requires an accurate knowledge of the scattering cross-sections. These cross-sections can be calculated by the quanto-mechanical laws described in the previous sections but require a lot of computer time for the calculations. Thus, extensive tabulations of all the scattering cross-sections can be useful for applications in Monte-Carlo calculations.

The accuracy of our numerical codes, utilized to compute all the scattering cross-sections reported below (*cf.* figures and tables) has been tested by comparing selected results to the available experimental data and numerical or analytical data from authors [8,10–17] who have investigated inelastic and elastic scattering of electrons in oxides.

Comparisons with experimental data concerning the relevant quantities (inelastic mean-free path, stopping power and differential elastic scattering cross-section) are presented in Figures 1 to 4. Comparison with experimental and theoretical data from other authors can also be found in our previous papers [18–24]. In any case, generally good agreement has been found, the inaccuracies with respect to the available experimental data being less than $\sim$ 5–15%, namely within the experimental errors: our numerical codes are thus appropriate to provide different cross-sections (*cf.* Tabs. 1 to 4) for use in Monte-Carlo calculations.

Concerning the inelastic mean-free paths (*cf.* Figs. 1 and 2), our present calculation provides values lower than those given by Ashley and Anderson [8] and by Tanuma *et al.* [13]. The differences can be attributed to the different data utilized for the optical loss function calculation. However the averaged experimental values are in better agreement with our calculation.

Table 5. Backscattering coefficient for electrons impinging on MgO, SiO_2, and Al_2O_3.

E (eV)	MgO	SiO_2	Al_2O_3
1 000	0.216	0.212	0.217
2 000	0.175	0.167	0.174
3 000	0.158	0.157	0.158
4 000	0.146	0.148	0.146
5 000	0.140	0.143	0.140
6 000	0.135	0.139	0.138
7 000	0.132	0.134	0.133
8 000	0.129	0.133	0.134
9 000	0.128	0.129	0.129
10 000	0.126	0.129	0.128

For the stopping power we find good agreement with experimental data (differences are less than $\sim 5\%$) when the electron energies are higher than 100 eV (*cf.*, for example, Figs. 3 and 4). A very good agreement (differences less than 1%) has also been found (over the whole energy range) by comparing our calculations for SiO_2 with those of Ashley and Anderson [8]. The discrepancy between theoretical calculation and experimental data for electron energies lower than 100–200 eV (Figs. 3 and 4) may be attributed to the not well experimentally established values of the imaginary part of the dielectric function for low energy (*cf.* Sect. 2).

Concerning the elastic cross-section, we have neglected here solid-state effects. For a discussion of these effects see, for example, reference [20]. We have also neglected charge-cloud polarization effects that are important when the electron energies becomes lower than $\sim$ 200–300 eV. Despite the neglect of solid-state and charge-cloud polarization effects, we see that our differential and transport cross-sections are accurate to within $\sim$ 1–2% when compared to the experimental data from other authors [16,17]. Larger errors ($\sim$ 5–15%, also depending on the electron kinetic energy) are expected for the total elastic scattering cross-section and the differential cross-sections when the scattering angles are lower than $\sim$ 5 degrees [25].

The Monte-Carlo procedure utilized for the backscattering coefficient calculations reported in Table 5 has been described in references [22,23]. The backscattering coefficient is defined as the fraction of electrons of the primary beam which, after a number of elastic and inelastic collisions with the atoms of the solid, emerge from the sample surface. The secondary electrons are not considered. For the present calculation the number of trajectories for each backscattering coefficient computation was 40 000 and every electron was followed into the solid target until its energy became lower than 50 eV. The values of the backscattering coefficient obtained for the three oxides and their trend as a function of the primary energy are very similar to that of a compound material whose average atomic number is ~ 10.

5 Conclusion

In this paper both the inelastic and elastic cross-sections of an electron beam interacting with MgO, SiO_2, and Al_2O_3 have been calculated. Comparing our results to experimental data for electrons interacting with our selected oxides, an accuracy better than $\sim$ 5–15% is found. Tabulations are provided for all quantities which describe the scattering of electrons in these oxides and which are relevant to Monte-Carlo simulation codes. Our Monte-Carlo simulation obtained by utilizing the present cross-sections permitted to calculate backscattering coefficients for the three oxides which decreases from ~ 0.22 to ~ 0.13 within the primary energy range of 1–10 keV.

References

1. J.C. Ashley, J. Electron. Spectrosc. Relat. Phenom. **46**, 199 (1988).
2. B.L. Henke, P. Lee, T.J. Tanaka, R.L. Shimabukuro, B.K. Fujikawa, At. Data Nucl. Data Tab. **27**, 1 (1982).
3. S.-R. Lin, N. Sherman, J.-K. Percus, Nucl. Phys. **45**, 492 (1963).
4. P.J. Bunyan, J.-L. Schonfelder, Proc. Phys. Soc. **85**, 455 (1965)
5. N.F. Mott, Proc. R. Soc. Lond. Ser. **124**, 425 (1929).
6. J.B. Furness, I.E. McCarthy, J. Phys. B **6**, 2280 (1973).
7. L. Pages, E. Bertel, H. Joffre, L. Sklavenitis, At. Data **4**, 1 (1972).
8. J.-C. Ashley, V.E. Anderson, IEEE Trans. Nucl. Sci. **NS28**, 4132 (1981).
9. J. Baró, J. Sempau, J.M. Fernández-Varea, F. Salvat, Nucl. Instrum. Meth. B **100**, 31 (1995).
10. F.L. Battye, J.K. Jenkin, J. Liesegang, R.C.G. Leckey, Phys. Rev. B **9**, 2887 (1974).
11. R. Flitsch, S.I. Raider, J. Vac. Sci. Technol. **12**, 305 (1975).
12. A. Ishizaka, S. Iwata, Y. Kamigaki, Surf. Sci. **84**, 355 (1979).
13. S. Tanuma, C.J. Powell, D.R. Penn, Surf. Interf. Anal. **17**, 927 (1991).
14. A. Akkerman, T. Boutboul, A. Breskin, R. Chechik, A. Gibrekhterman, F. Lifshitz, Phys. Stat. Sol. (b) **198**, 769 (1996).
15. D.C. Joy, Scanning **17**, 270 (1995).
16. J.P. Bromberg, J. Chem. Phys. **52**, 1243 (1970).
17. R.D. Dubois, M.E. Rudd, J. Phys. B: At. Mol. Phys. **9**, 2657 (1976)
18. M. Dapor, Nucl. Instrum. Meth. B **95**, 470 (1995); *ibid.* **108**, 363 (1996).
19. M. Dapor, J. Appl. Phys. **77**, 2840 (1995).
20. M. Dapor, J. Appl. Phys. **79**, 8406 (1996).
21. M. Dapor, A. Miotello, Phys. Rev. B **56**, 2234 (1997).
22. A. Miotello, M. Dapor, Phys. Rev. B **56**, 2241 (1997).
23. M. Dapor, A. Miotello, Surf. Interf. Anal. **26**, 531 (1998).
24. M. Dapor, A. Miotello, At. Data Nucl. Data Tab. **69**, 1 (1998).
25. M. Riley, C.J. MacCallum, F. Biggs, At. Data Nucl. Data Tab. **15**, 443 (1975).